

Proximity Prediction of Mobile Objects to Prevent Contact-Driven Accidents in Co-Robotic Construction

Daeho Kim¹, SangHyun Lee², and Vineet R. Kamat³

Abstract

7 Robotic solutions have garnered increased attention from the construction industry as an effective
8 means of improving construction safety and productivity. However, in deploying such robots to real
9 fields many safety concerns have remained untackled, particularly contact-driven accidents that can be
10 potentially escalated by mobile robots. To address this issue, the authors develop a fully automated
11 framework that enables predicting the proximity between mobile objects, leveraging a camera-mounted
12 unmanned aerial vehicle (UAV), computer vision, and deep neural networks, and conduct a field test to
13 evaluate its validity. In the test, the framework showed a promising result: it achieved average proximity
14 error of 0.95 meters in predicting 5.28 seconds future proximity between a worker and a truck. The
15 major contribution of this study is in predicting the risk of impending collision in advance, thereby
16 making pro-active interventions possible. Computationally, the predictive functionality based on
17 computer vision and deep neural network including convolutional neural network and generative
18 adversarial network would allow robots to examine alternative multiple paths beforehand and enable
19 providing advance alerts to workers. These pro-active interventions would effectively reduce the
20 chances of impending collisions between mobile robots and construction workers.

22 **Keywords:** Autonomous robot; Contact-driven accident; Proximity prediction; Unmanned aerial
23 vehicle; Deep neural network.

¹ Ph.D. Candidate, Dept. of Civil and Environmental Engineering, Univ. of Michigan, MI, 48109.

² Professor, Dept. of Civil and Environmental Engineering, Univ. of Michigan, MI, 48109, E-mail: shdpm@umich.edu. (Corresponding author)

³ Professor, Dept. of Civil and Environmental Engineering, Univ. of Michigan, MI, 48109.

24 **Introduction**

25 Construction industries around the world are gradually gearing up for robotic automation (Tsuruta et al.
26 2019; Lattanzi and Miller 2017; Veha et al. 2013). A growing number of construction companies are
27 embracing robotic solutions to reap the benefits of improved productivity and safety (Kim et al. 2019a;
28 Bock 2015). Notably, the global construction robot market is rapidly growing; it is expected to reach
29 around \$190 million by 2025, at a compound annual growth rate (CAGR) of over 20% (Research and
30 Market 2019). According to a market report from Tractica, U.S., more than 7,000 autonomous (or semi-)
31 robots are expected to be deployed to construction fields in the U.S. between 2018 and 2025 (Tractica
32 2019).

33 A wide range of construction robots are under development or in the early stage of deployment:
34 for example, to name a few, there are structure robots for 3D printing (Liu and Li 2018), bricklaying
35 (Moon et al. 2018), welding (Tavares et al. 2019), modular building (Yang et al 2019), finishing robots
36 for drywall installation (Yu et al. 2016), façade painting and cleaning (Vega-Heredia et al. 2019), and
37 infrastructure robots for demolition (Li et al. 2019; Zheng et al. 2018), and rebar tying (Cardno 2018).
38 Assisting physically demanding, highly repetitive, and hazardous tasks in construction, such robots are
39 expected to be the main driver that transforms future construction into a more productive and safer
40 industry.

41 However, in deploying such robots to real fields, many safety concerns have remained
42 untackled (Guiochet et al. 2017). The authors specifically cast light on the contact-driven hazards that
43 could be escalated by mobile robots. Construction generally takes place in a highly unstructured and
44 dynamic environment. Workspace (e.g., terrain and structure) evolves over time and multiple entities
45 (e.g., workers, equipment, and robots) are bound to share a limited workspace. In such a unstructured
46 and evolving space, the chances of contact-driven accidents (e.g., struck-by and caught-in/between) by
47 motorized resources can arise easily, frequently, and unexpectedly (Kim et al. 2019b; Teizer et al. 2010).

48 In co-robotic construction, where mobile robots are closely involved in the field built for
49 human labor, workers will be assuming greater risk for such accidents. Any movement caused by
50 misperception of a situation (e.g., approaching, deviating, and reversing) can pose a fatal threat to

51 nearby workers. However, it is unknown how mobile robots' situational intelligence—such as the
52 capacity for understanding, reasoning, and improvisational decision making—rises to the dynamically
53 evolving situations of construction. In mobile robots' navigation and behavior in such uncertain
54 situations, there could be unexpected errors, which could pose a greater risk of forcible contact to nearby
55 workers.

56 A major research question for this problem has been attuned to the process of detecting the
57 proximity between workers and robots (or mobile equipment) in time (Kim et al. 2019b; Park et al.
58 2016; Teizer 2015; Teizer et al. 2010). Several collision avoidance technologies, such as those using
59 proximity sensors or computer vision methods, have been explored to this end. Most existing
60 technologies have been used to monitor or detect the proximity at a current time-step, relying upon
61 present sensory data. In many cases, however, prediction is far more important and effective for contact-
62 driven accident prevention (Kim et al. 2019c). This is principally because the sooner robot and worker
63 are informed of their proximity to each other, the more likely they are to avoid the potential collision.
64 Nevertheless, few studies have attempted to address it.

65 With this background, the authors develop deep neural networks (DNNs)-based framework
66 that enables proximity prediction of mobile objects. In this framework, a camera-mounted unmanned
67 aerial vehicle (UAV) monitors associated entities, serving as the third eye of robots and workers, which
68 has a wider line-of-sight (Figure 1). Inputting the UAV-captured imagery data, the framework powered
69 by DNNs for object detection (Figure 1-A) and trajectory prediction (Figure 1-B) performs proximity
70 prediction (Figure 1-C) in a fully automated way.

71 The major contribution of this work is to enable predicting the risk of impending collision in
72 advance, thereby making pro-active safety interventions possible. Specifically, the proximity prediction
73 would assist mobile robots' predictive path planning and rerouting. Also, via wearable devices (e.g.,
74 wrist band and smart safety glasses), it would enable providing an advance alert to workers, helping
75 them to take timely evasive action. These pro-active interventions would effectively reduce the chances
76 of impending collisions between mobile robots (or mobile equipment) and construction workers.

77 Moreover, the authors apply a generative adversarial network (GAN) to trajectory prediction, which
78 opens a new possibility of GAN for potential construction applications.

79

80 **Existing Collision Avoidance Technologies and Challenges in Construction Applications**

81 There has been a wide range of collision avoidance technologies, such as those based on proximity
82 sensors or computer vision methods. This section provides a holistic view of these technologies,
83 discussing their pros and cons. In addition, the authors detail a major challenge that the technologies
84 would have in construction field applications.

85

86 ***Collision Avoidance Technologies: Proximity Sensors***

87 Based on operation principles, proximity sensors can be largely categorized into two types: (i) time-of-
88 flight (TOF)-based sensor and (ii) tag-based sensor. The TOF-based sensor, installed on a robot,
89 measures the distance of surroundings (e.g., geographic features, obstacles, and workers) by emitting a
90 certain form of energy and reading its time-of-flight. As well-recognized sensors, sound navigation and
91 ranging (SONAR), radio detection and ranging (RADAR), and light detection and ranging (LIDAR)
92 are included in this category.

93 SONAR (or ultrasonic sensor) measures distances to physical objects by transmitting a high-
94 frequency sound wave and measuring the TOF of its echo reflected from the target objects. A sound
95 wave requires a certain medium to travel. Its propagation, therefore, involves many disturbances by the
96 medium's physical conditions (e.g., temperature and pressure), and it can be more so particularly in the
97 case of longer-range detection (Varghese and Boone 2015). Accordingly, the application of SONAR in
98 mobile robots has been limited to short-range detection—typically less than 3 meters (e.g., reverse
99 parking) (Ducarme 2019).

100 On the other hand, RADAR uses radio signal (300 MHz - 40 GHz), a kind of electromagnetic
101 wave, which does not require a certain medium to travel. It thus functions in many wild conditions (e.g.,
102 rain, fog, snow, and dust) and has a long-range of reading—generally more than 30 meters (Ducarme
103 2019). In addition, using Doppler Effect (Chen et al. 2006), it can also detect the speed of moving

104 objects as well as its proximity (Varghese and Boone 2015). However, the performance of RADAR can
105 vary by reflectors. This is because the radio signal can be easily dispersed, particularly when
106 encountering unfavorable reflectors such as plastics, dry wood, or objects with large flat surfaces (Ruff
107 2006).

108 LIDAR also uses a kind of electromagnetic wave, the beam of light (or laser). It is able to not
109 only measure distances to objects but also scan 3D surroundings with multi-axis lasers. The more lasers
110 a LIDAR transmits, the denser 3D world can be reconstructed (Ducarme 2019; Varghese and Boone
111 2015). Of stand-alone sensors, LIDAR is often cited as the most accurate proximity sensor (Gargoum
112 et al. 2018). Also, the 3D readout is potentially used as the primary source for the path planning of many
113 autonomous navigating robots (Kim et al. 2018). However, LIDAR, as with other TOF-based sensors,
114 cannot distinguish what the detected objects are. To distinguish objects, it needs additional object
115 classification software (Ducarme 2019).

116 Distinctive to these TOF-based sensors, tag-based sensors utilize an energy field (e.g.,
117 electromagnetic field) and detect proximity via the signal communication between a reader mounted to
118 a robot and tags worn by workers. With this principle, many kinds of sensors have been devised,
119 including radio frequency identification (RFID), magnetic field (MF), and Bluetooth low energy (BLE).
120 As the tag-based sensors don't rely on the TOF measurement, they are less affected by the line-of-sight
121 (Ducarme 2019). However, the tag-based sensors have hardly gained a competitive edge over the TOF-
122 based sensors in terms of accuracy and fidelity. According to a test conducted by Park et al. (2016), the
123 proximity errors of RFID, MF, and BLE sensors were up to 5.0, 3.4, and 2.6 meters, respectively, with
124 the standard deviation of 2.1, 0.3, and 1.8 meters. Although the tag-based sensors still have the potential
125 to complement other technologies (e.g., SONAR, RADAR, and LIDAR), the prerequisite that all targets
126 need to be attached with a tag hinders their application in construction (Memarzadeh et al. 2013; Park
127 et al. 2012).

128 The proximity sensors have been widely applied in robotics to assist the robots' collision
129 avoidance (Cui et al. 2019). However, the effectiveness, availability, and functionality of the existing
130 proximity sensors could be challenged in a highly unstructured and dynamic construction site. For

131 example, the TOF-based sensors (e.g., SONAR, RADAR, and LIDAR) could be frequently blinded by
132 physical barriers; while the performances of tag-based sensors (e.g., RFID, MF, and BLE) are
133 susceptible to deterioration due to the jamming caused by metallic or wooden objects, both of which
134 are common in construction sites.

135 Above all, this study highlights the existing technologies' limited scope of application in
136 construction. The application of sensor-based technologies have been limited to detecting or monitoring
137 proximity at current time-step. However, it may not be as effective in many impending situations. In a
138 dynamic and unstructured construction site, contact-driven accidents occur spontaneously in
139 unexpected ways. In such an impending situation, mere detecting or monitoring proximity would not
140 be effective because the near-sighted measure wouldn't allow enough time for the involved robot (and
141 equipment operator) and worker to take prompt evasive action. In this sense, to better prevent contact-
142 driven accidents in co-robotic construction, collision avoidance technology needs to be equipped with
143 the prediction functionality for potential accidents.

144

145 ***Collision Avoidance Technologies: Computer Vision-based Methods***

146 Over recent years, computer vision-based methods have demonstrated great potential as a
147 supplementary technology to proximity sensors (Zhu et al. 2017; Park et al. 2016; Memarzadeh et al.
148 2013; Park et al. 2012; Brilakis et al. 2011). It uses one or more imaging devices (e.g., digital camera)
149 to capture multiple targets and stream the digital images to a computer. In turn, it utilizes the computing
150 power to conduct object detection and proximity measurement. With the improvement of computing
151 power, the potential of the computer vision continues to grow. This growth is evidenced by the number
152 of construction studies that have explored computer vision-based collision avoidance technologies. For
153 example, Memarzadeh et al. (2013) developed an algorithm to detect multi-class construction objects
154 by integrating histogram of oriented gradient (HOG) and histogram of hue-saturation-value (HSV);
155 Kim et al. (2016) proposed a proximity monitoring framework that employs Gaussian mixture model
156 (GMM)-based object detection; Kim et al. (2017) introduced another proximity monitoring framework
157 using multi-view cameras and object detection based on HOG and support vector machine (SVM). The

158 previous studies have greatly contributed to examining the potential of computer vision-based collision
159 avoidance technologies. However, there are several drawbacks of the computer vision-based methods,
160 which need to be addressed for construction applications.

161 A major imaging device widely used is stationary cameras such as tripod-mounted or
162 surveillance cameras (Zhu et al. 2017; Park et al. 2016; Brilakis et al. 2011). These cameras are cheap,
163 readily available, and easy to apply. However, this technology can involve frequent occlusions of targets
164 (i.e., the situation that targets are occluded by physical barriers and so become invisible) particularly on
165 construction sites where a number of obstacles to the camera's line-of-sight are scattered (Kim et al.
166 2019b). The problem is that such occlusions are fatal to any computer vision-based object detection
167 because the computer vision is bound to rely on the visible information of a target (e.g., the target's
168 pixel values and configuration). Therefore, the application of mobile imaging devices which have a
169 wider line-of-sight and mobility, thereby reducing such occlusions (e.g., UAVs), must be considered.

170 Many earlier studies applied one or more hand-crafted features—such as HOG, HSV, scale
171 invariant feature transform (SIFT), and speeded-up robust features (SURF)—to object detection.
172 However, using such features naturally involves a heavy computation due to pre-processing and
173 multiple steps for feature extraction, resulting in slow processing speed (Kim et al. 2019b). Recently,
174 DNN-based object detection has made large progress in terms of speed and accuracy by leveraging
175 parallel computing and finer-level learned features. Accordingly, an increasing number of studies have
176 attempted to apply the DNN-based object detection framework for construction applications. For
177 example, Fang et al. (2018), Luo et al. (2018), Son et al. (2019), and Yan et al. (2019) applied faster
178 region-based convolutional neural network (Faster R-CNN, Ren et al. 2017) for construction objects
179 detection; Kim et al. (2018) and Alipour et al. (2019) applied region-based fully convolutional network
180 (R-FCN, Dai et al. 2016). The studies applying DNNs proved to greatly improve the speed and accuracy
181 of construction object detection. However, since the DNNs (i.e., Faster R-CNN and R-FCN) rely on
182 two-stage inferences (region proposal and classification) by two separated networks, they involve a
183 high computational cost and couldn't achieve the real-time operation—30 frame per second (*FPS*). The

184 real-time operation is definitely critical in assisting collision avoidance. Computer vision-based
185 methods, therefore, must demonstrate real-time operation for real-world applications.

186 Despite the drawbacks, computer vision-based methods have immense potential to supplement
187 sensor-based technologies. With increasingly published vision datasets, advanced DNN architectures,
188 and enhanced computing power, both speed and accuracy of computer vision-based methods continue
189 to improve. Also, it involves less hardware installation and enables classification as well as the detection
190 of multiple objects. However, its scope of application, as with the aforementioned sensor-based
191 technologies, has been limited to proximity monitoring at current time-step. To more pro-actively assist
192 collision avoidance, the prediction of future proximity and potential hazard needs to be addressed.

193

194 **DNN-based Framework for Proximity Prediction**

195 To address the above challenges, the authors develop a fully automated framework that enables real-
196 time proximity prediction of mobile objects, leveraging a camera-mounted UAV, object detection DNN
197 [you only look once-v3 (YOLO-V3, Redmon and Farhadi 2018)], and trajectory prediction DNN [social
198 GAN (S-GAN, Gupta et al. 2018)]. This framework consists of two main modules: (i) a trajectory
199 observation module that monitors targets' locations and records their past trajectories and (ii) a
200 trajectory prediction module that predicts the target's future trajectories and estimates their future
201 proximity. This section details each module's functionality and development process as well as presents
202 its validation result.

203

204 ***Module 1: Trajectory Observation***

205 The first module monitors targets' locations and records their past trajectories, which are the primary
206 input for trajectory prediction (Figure 2). This module first detects targets on a UAV-captured input
207 image and estimates their center location as image coordinates (i.e., x-y pixel coordinates) using an
208 object detection model based on YOLO-V3 (Figure 2-A). In turn, this module rectifies the coordinates
209 to the world coordinates through geometric transformation using a reference object since the image
210 coordinates can neither reflect the true scene scale nor be accurate due to a projective distortion inherent

211 on a 2D image captured by a UAV (Figure 2-B). This module runs the object detection and the
212 coordinate rectification at every input image, thereby continuing to update true-to-scale, distortion-free
213 locations of targets. Based on the location information, it records the targets' past trajectories (from 3.96
214 seconds earlier to current, Figure 2-C) and streams those to the second module for trajectory prediction.

215 The primary role of Module 1 is the trajectory observation of mobile construction objects but
216 it can also conduct real-time proximity monitoring. In a prior study (Kim et al. 2019b), the authors
217 demonstrated this module's performance on proximity monitoring—0.26 meters average displacement
218 error (i.e., average of Euclidean distance between a target's ground truth and estimated positions) and
219 0.61 meters average proximity error (i.e., average of absolute difference between a pair of targets'
220 ground truth proximity and estimated proximity). The details of Module 1's proximity monitoring
221 performance can be found in our prior study (Kim et al. 2019b).

222

223 **Object Detection using YOLO-V3**

224 To develop an object detection model, the authors leveraged YOLO-V3, which demonstrated
225 outstanding performances in terms of both speed and accuracy. The YOLO-V3 realizes a one-stage
226 operation by leveraging end-to-end convolutional layers and grid-based value encoding. As a result, it
227 could reduce the network complexity and computational cost, achieving real-time operation (35 *FPS*)
228 (Redmon and Farhadi 2018). Also, taking advantage of multi-scale inference, the YOLO-V3 improves
229 reasoning capability. Consequently, it could show superior accuracy on common objects in context
230 (COCO) object detection challenge [55.3% mean average precision (*mAP*)] over other one-stage object
231 detection DNNs [e.g., single shot multibox detector (SSD, Liu et al. 2016): 45.4% *mAP* and
232 deconvolutional single shot detector (DSSD, Fu et al. 2017): 46.1% *mAP*] (Redmon and Farhadi 2018).

233 In this work, the authors started from a YOLO-V3 model developed in our prior study (Kim
234 et al. 2019b) which was trained with COCO (Lin et al. 2014) and construction dataset ($N=4,114$) and
235 updated through additional fine-tuning with larger construction dataset ($N=13,147$). As a result, the
236 updated model demonstrated a promising detection performance on a test dataset ($N=547$): it showed
237 97.23% *mAP* (Equation 1) and 83.54% average intersection over union (Avg. *IoU*, Equation 2) for

238 excavator, wheel loader, truck, worker, and reference objects (e.g., square, rectangular, and pentagonal
239 concrete footings).

240 While it would have been ideal to train this model with a mobile construction robots dataset
241 as well, the lack of imagery data for mobile construction robots made such work impossible to complete
242 at this time. This model would have another chance to fine-tune its process once sufficient datasets for
243 mobile construction robots become available.

244

$$mAP = \frac{1}{n} * \sum_1^n \left(\frac{1}{11} * \sum_{r=0.0,0.1,\dots,1.0} MP_r \right) \quad \text{Equation 1}$$

Note: n=the total number of object classes; MP_r=maximum precision at a certain recall value r (i.e., 0, 0.1, 0.2, ..., 1.0) on precision-recall curve of 50% IoU.

245

$$\text{Avg. IoU} = \frac{1}{k} * \sum_1^k \left(\frac{AoO}{AoU} \right) \quad \text{Equation 2}$$

Note: k=the total number of detected objects; AoO=area of overlap; AoU=area of union.

246

Coordinate Rectification using Geometric Transformation

248 While a camera maps a 3D world onto a 2D image, the real scene scale is lost and a projective distortion
249 arises (Figure 2-B). Therefore, the image coordinates of an object can neither reflect the true scene scale
250 nor be accurate. Module 1 thus performs coordinate rectification following the object detection, thereby
251 recording true-to-scale, distortion-free coordinates of objects. To this end, this module uses a geometric
252 transformation algorithm using a reference object, which was developed in our prior study (Kim et al.
253 2019b). This algorithm detects a reference object's edges, contours, and four vertexes and estimates the
254 transformation matrix by matching the vertexes to the known reference dimensions (Figure 2-B). In
255 turn, it converts image coordinates to true-to-scale, distortion-free world coordinates using the
256 transformation matrix. In a prior study (Kim et al. 2019b), the authors validated the effect of the

257 geometric transformation algorithm on improving distance measurement accuracy: in a lab test, the
258 algorithm improved the percentage accuracy of proximity measurement from 68.32% to 93.33% at the
259 maximum. The details of the geometric transformation algorithm and its evaluation result can be found
260 in our prior study (Kim et al. 2019b).

261 Figure 2 illustrates an example of the geometric transformation where a square concrete
262 footing is used as a reference object (Figure 2-B). However, any objects having four or more vertexes—
263 such as quadrangle, pentagonal, or hexagonal objects—can be used as a reference object if its
264 dimensions are known.

265

266 ***Module 2: Trajectory Prediction***

267 The second module (i.e., trajectory prediction) takes a set of target's past trajectories as input (from
268 3.96 seconds earlier to current, Figure 3-A) and predicts their future trajectories for up to 5.28 seconds
269 (Figure 3-B), using a trajectory prediction model based on S-GAN. The set of future trajectories informs
270 where the targets will be located for the next 5.28 seconds at an interval of 0.66 seconds. Lastly, based
271 on the targets' predicted locations, this module estimates the targets' proximity for the next 5.28
272 seconds—the proximity after 0.66, 1.32, 1.98, 2.64, 3.30, 3.96, 4.62, and 5.28 seconds (Figure 3-C).

273 Trajectory prediction studies have been dominated by data-driven learning approaches. This
274 is basically because the movement of an entity (e.g., people) is so diverse and uncertain that it is
275 extremely challenging to model through hand engineering. In an early stage, there are several studies
276 to use hand-crafted features-based learning (Yamaguchi et al. 2011; Antonini et al. 2006; Helbing and
277 Molnar 1995) or statistical learning such as polynomial regression (Rashid and Behzadan 2017),
278 Gaussian process (Trautman et al. 2015; Tay and Laugier 2008), and hidden Markov model (Rashid
279 and Behzadan 2017). However, many contemporary studies are motivated to use a DNN, following the
280 trajectory of many other data-driven studies. In recent years, several DNN architectures for trajectory
281 prediction have been released: for example, there are social long short-term memory (S-LSTM, Alahi
282 et al. 2016), crowd interaction DNN (Xu et al. 2018), interaction aware DNN (Pfeiffer et al. 2018), and
283 S-GAN (Gupta et al. 2018). Of these, the S-GAN, incorporating several distinctive features,

284 demonstrated a state-of-the-art performance over others (Gupta et al. 2018). It enables a model to learn
285 social behavior (e.g., collision avoidance) as well as an entity's moving pattern by integrating an LSTM
286 encoder-decoder and a social pooling layer (Gupta et al. 2018). By realizing GAN architecture (i.e.,
287 coupling discriminator to generator) and adversarial training, it enhances the capability to learn
288 complicated distributions of mobile objects' trajectories and improves reliability of prediction output.
289 For this reason, this study applied the S-GAN and developed a trajectory prediction model through
290 transfer learning.

291

292 **Network Architecture of S-GAN**

293 The S-GAN has two main components: (i) generator that predicts targets' future trajectories (Figure 4-
294 A) and (ii) discriminator that inspects the quality of the predictions (Figure 4-B).

- 295 • Generator (Figure 4-A): the generator takes past trajectories of targets as input and predicts their
296 future trajectories through network integrating social pooling layer into the middle of LSTM
297 encoder-decoder. The generator first converts the input trajectories to fixed-length vectors via
298 multilayer perceptron (MLP, Figure 4-AA) and feeds it to LSTM units of encoder (figure 4-AB).
299 The LSTM units then encode the targets' movement patterns individually and forward the encoded
300 features to social pooling layer which infers the targets' social interactions and generates pooled
301 tensor for each target (Figure 4-AC). Lastly, the decoder interprets the interconnected hidden state
302 of input trajectories with multiple LSTM units and generates socially plausible future trajectories
303 of the targets (Figure 4-AD). Here, the decoder initializes itself with input trajectories so that it can
304 generate future trajectories that better conform to the past ones.
- 305 • Discriminator (Figure 4-B): the discriminator inspects the predicted trajectories' quality and
306 conformity to the past trajectories. It takes both of past and future trajectories together as input and
307 encodes their conformity features through LSTM units (Figure 4-BA). In turn, it calculates the
308 predicted trajectories' conformity score via MLP (Figure 4-BB) and inspects them whether they are
309 plausible or not (i.e., classifies whether real or fake). The prediction that successfully fools the
310 discriminator is selected as the final outcome.

311 **Transfer Learning of S-GAN**

312 The authors developed a trajectory prediction model through transfer learning of the S-GAN. The
313 following details were specifically considered: (i) parameter initialization, (ii) fine-tuning, and (iii)
314 hyper-parameter tuning. This work started from the S-GAN model, which is pre-trained with the two
315 benchmark datasets: (i) Eidgenossische Technische Hochschule Zurich (ETH, Pellegrini et al. 2010)
316 and (ii) University of Cyprus (UCY, Leal-Taixe et al. 2014). As the most widely benchmarked datasets
317 in trajectory prediction studies, the two datasets in total contain 1,536 human trajectories. They reflect
318 various movement patterns such as crossing each other, collision avoidance, group forming, and
319 dispersing (Alahi et al. 2016). Having such diverse data in pre-training was intended to prevent
320 overfitting in the following fine-tuning process.

321 From that starting point (i.e., pre-learned weights), the fine-tuning with construction dataset
322 was conducted to better fit the pre-trained model to construction settings. Specifically, the authors fine-
323 tuned it with the integrated dataset (i.e., ETH + UCY + the construction dataset), rather than only with
324 the construction dataset, so as to minimize the possibility of overfitting. In this tuning, the trajectories
325 of construction mobile resources (e.g., worker, wheel loader, and excavator), annotated from 916 UAV-
326 captured images, were used.

327 The farther prediction is achieved, the earlier safety intervention can be made. The authors
328 thus modified the original prediction length (3.96 seconds=12 time-steps x 0.33 seconds) to 5.28
329 seconds (16 time-steps x 0.33 seconds) and particularly examined how observation-related hyper-
330 parameters affects the model's final performance. Trajectory prediction is primarily based on the
331 interpretation of targets' previous movement patterns. Thus, the properties of past trajectory must have
332 a significant impact on the model's final performance. In this sense, this task additionally tuned the two
333 observation-related hyper-parameters (i.e., observation length and sampling interval) with the following
334 reasons.

335 • Observation length: a target's future trajectory is highly attributed to its previous movement pattern.
336 The length of observation (i.e., how long observation the model will consume) must thus have a
337 significant impact on a model's prediction performance. Thus, three different observation lengths

were considered in this work: (i) 2.64 seconds (80 frames), (ii) 3.96 seconds (120 frames), and (iii) 5.28 seconds (160 frames).

- Sampling interval: the other hyper-parameter selected was sampling interval. This is because it controls the minuteness of input and output trajectories. With a denser sampling interval, the model can have finer input, but should take the burden of outputting denser prediction as well. On the other hand, with a sparser sampling interval, the model should have coarser input but can avoid such complexity. To examine which level of sampling interval would better fit for our problem, the authors considered four different sampling intervals: (i) 0.17 seconds (5 frames), (ii) 0.33 seconds (10 frames), (iii) 0.66 seconds (20 frames), and (iv) 1.33 seconds (40 frames).

Test Result

For comparative evaluation of the twelve tuned models, the test on a construction dataset was followed. In this test, a total of 397 UAV-captured images was used and the trajectories of three object classes were considered: (i) worker, (ii) wheel loader, and (iii) excavator (Figure 5). As evaluation metrics, average displacement error (*ADE*) and final displacement error (*FDE*), the typical two evaluation metrics to access trajectory prediction accuracy, were applied (Alahi et al. 2016; Gupta et al. 2018). The *ADE* is the average value of displacement errors (*DEs*, Euclidean distances) between ground truths and predictions over all predicted time-steps (i.e., average of *DE@1st~8th*, Figure 5) meanwhile the *FDE* is the distance between the predicted final destination and the ground truth destination at the end of the prediction period (i.e., *DE@8th*, Figure 5). This test was intended to evaluate the pure performances of the tuned models, so the authors fed the models the ground truth of observation trajectories.

Table 1 summarizes the *ADE* and *FDE* results. Overall, the tuned models showed a promising prediction accuracy: all the *ADEs* were less than 0.9 meters and the *FDEs* were less than two meters. It was shown that the model of 0.66 seconds (20 frames) sampling interval and 3.96 seconds (120 frames) observation length has the highest accuracy in terms of both *ADE* and *FDE*: this model achieved the *ADE* of 0.45 meters and the *FDE* of 0.79 meters in this test. Considering this result, the authors adopted the model that showed the least error as the trajectory prediction module.

365 **Field Test**

366 A field test was conducted to demonstrate the validity of the overall framework. It would have been
367 ideal to test the proposed framework with mobile construction robots, since the robots are hardly
368 available to date, this test employed a truck which is similar looking to an autonomous truck. Figure 6
369 illustrates the test environments and settings. In this test, the authors simulated the three types of
370 movement patterns between a worker and a truck: (i) moving forward side by side (movement pattern
371 #1); (ii) crossing each other side by side (movement pattern #2); and (iii) crossing each other in curves
372 (movement pattern #3), as shown in Figure 6. The worker and the truck set off at the same time at the
373 designated origins and followed the ground lines at a constant velocity (*1.5 meters/second*) until arriving
374 at the designated destinations. The movement patterns were simulated three times per each. During this
375 test, the authors flew a camera-mounted UAV over the testbed and ran the developed framework to
376 predict the proximity between the targets (i.e., the metric distance between the worker and the truck).
377 Lastly, the accuracy of the proximity outputs was evaluated by comparing it to the corresponding ground
378 truth proximity.

379

380 **Measurement of Ground Truth Proximity**

381 To measure the ground truth proximity over all time-steps, the authors intentionally used ground lines
382 and markers (Figure 6). The targets were ordered to follow a reference line at a constant velocity.
383 Therefore, the origin-destination locations and times of a target were known so that the target's in-
384 between locations and times could be measured by interpolation. In doing so, the authors measured all
385 the ground truth locations of the targets over all time-steps and their ground truth proximity accordingly.

386

387 **Evaluation Metrics**

388 To evaluate the accuracy of targets' predicted locations, the two displacement errors, average
389 displacement error (*ADE*) and final displacement error (*FDE*), were applied. While the *ADE* and *FDE*
390 represent the accuracy of predicted trajectory for each individual target, it does not directly represent
391 the accuracy of predicted proximity between a pair of targets. Thus, in addition to the *ADE* and *FDE*,

392 this test also evaluated average proximity error (*APE*) and final proximity error (*FPE*). The *APE* is the
393 average value of the absolute differences between predicted proximity and ground truth proximity over
394 all time-steps (Equation 3). Meanwhile, the *FDE* is the absolute difference between predicted proximity
395 and ground truth proximity at the end of the prediction period (Equation 4). Lastly, this test also
396 measured each module's operating time to evaluate its computational efficiency.

397

$$APE = \frac{1}{n} * \sum_{i=1}^n |P_g - P_p| \quad \text{Equation 3}$$

Note: n=the number of cases; P_g=ground truth proximity; P_p=predicted proximity.

$$FPE = |P_{gf} - P_{pf}| \quad \text{Equation 4}$$

*Note: P_{gf}=ground truth proximity at the end of prediction period (i.e., after 5.28 seconds);
P_{pf}=predicted proximity at the end of prediction period (i.e., after 5.28 seconds).*

398

399 **Proximity Prediction Result**

400 In terms of *ADE* and *FDE*, the developed framework showed promising results. Overall it achieved the
401 *ADEs* for both the worker and the truck less than two meters, the *FDEs* less than 3.5 meters (Table 2).
402 The *ADE* and *FDE* for the worker were 1.64 and 3.39 meters overall and those for the truck were 1.99
403 and 2.99 meters (Table 2). In line with the *ADE* and *FDE* results, the *APE* and *FPE* results were also
404 promising. Overall the framework achieved 0.95 meters *APE* and 1.71 meters *FPE* between the worker
405 and the truck (Table 3). Also, the *APEs* between the worker and the truck for all three movement patterns
406 were less than 1.5 meters, the *FPEs* less than 2.5 meters (Table 3).

407 Notably, it was determined that to predict farther time-step is more challenging. Figure 7
408 illustrates the trend of proximity error (i.e., absolute difference between predicted proximity and ground
409 truth proximity) as prediction time-step increases. As shown in Figure 7, for all movement patterns, the
410 proximity errors continued to rise as the prediction time-step increases: on average, the framework
411 showed the proximity error of 0.53 meters at 0.66 seconds prediction, but the error continued to climb

412 as prediction time-step went farther, reaching to 1.71 meters (=the overall *FPE*, Table 3) at 5.28 seconds
413 prediction (Figure 7).

414

415 **Operating Time**

416 Figure 8 illustrates the operating time of Modules 1 and 2. With a single graphic processing unit (GPU,
417 NVIDIA Tesla K40), Module 1 (i.e., trajectory observation) spent 0.28 seconds per a frame (Figure 8-
418 A) and Module 2 (i.e., trajectory prediction) spent 0.12 seconds per a cycle (i.e., from taking a set of
419 past trajectories to generating a set of future trajectories, Figure 8-B). Given that this framework runs
420 Module 1 at every 0.66 seconds (i.e., at 20 frames interval), it was able to perform trajectory observation
421 with zero time-lag in computation. And overall, the framework demonstrated that it can update the
422 future proximity for the next 5.28 seconds at every 0.66 seconds with 0.40 seconds time-lag in
423 computation (i.e., 0.28 seconds for Module 1 + 0.12 seconds for Module 2, Figure 8-C). It means that
424 the framework can update future proximity for the next 4.88 seconds at every 0.66 seconds continuously
425 (i.e., 5.28 seconds prediction – 0.40 seconds time-lag in computation).

426

427 **Discussions**

428 As shown in the field test, the developed framework demonstrated a promising performance of
429 proximity prediction in terms of both accuracy and speed. On the basis of the result, in this section, the
430 authors present how this framework can better assist the collision avoidance between workers and
431 mobile robots (or mobile equipment) at unstructured and dynamic construction sites. In addition, the
432 authors discuss the implication of using GAN-based trajectory prediction DNN and lastly present
433 potential improvement points for future studies.

434

435 ***Real-World Applications to Prevent Contact-driven Accidents by Mobile Objects***

436 The framework showed that it can continuously update future proximity for the next 5.28 seconds at
437 every 0.66 seconds within one-meter proximity error on average (computing time per update=0.40
438 seconds). This prediction performance can have a far-reaching significance beyond the detection of

439 current proximity in accident prevention in that it enables pro-active safety interventions. For example,
440 if a robot can be informed of whether a worker will be on the path or inside the action radius of itself in
441 the future, the robot can make pro-active path planning and rerouting in advance. Likewise, it is also
442 possible to provide an advance alert to workers via wearable devices (e.g., wrist band and smart safety
443 glasses) so that the workers can take timely evasive action. Assuming that an autonomous truck is
444 approaching a worker at five meters per second, the framework can inform the worker and the
445 autonomous truck of their potential collision 5.28 seconds before it happens. The worker then has
446 around 25 meters of physical distance from the autonomous truck to easily avoid the collision without
447 strain. These pro-active interventions would effectively reduce the chances of an impending collision
448 between mobile robots and construction workers.

449 In addition, the developed framework also can be readily applied to other mobile objects such
450 as motorized equipment and vehicle. This framework can detect mobile objects, such as excavator,
451 wheel loader, and truck, and also, the scope of targets can be easily expanded through tuning of the
452 object detection model with the additional training dataset. The framework can thus provide equipment
453 operators and vehicle drivers with an alert in advance as well, helping to avoid a potential collision with
454 workers and mobile robots.

455 In real-world applications, however, the quality and speed of network connection need to be
456 further investigated and improved. The developed framework uses a camera-mounted UAV (or UAVs)
457 to stream imagery input data to a computing device (e.g., a cloud server). Also, it needs wireless
458 communication with robots and wearable devices to timely feedback. Therefore, in real-world
459 applications, it is critical to ensure rapid data transmission from a computing device to a UAV (or UAVs),
460 wearable devices, and robots. Leveraging 5G wireless network and internet of thing (IoT) cloud
461 platform can be a promising solution to this end. The 5G wireless network would support real-time data
462 transmission at data transfer rate of several gigabytes per second. Also, with the high-speed network
463 connection, an IoT cloud platform could connect multiple UAVs, robots, and wearable devices to a
464 cloud server, which would enable near real-time operation of proximity prediction as well as rapid
465 communication with workers and robots.

466 To the fully automated operation of the proposed framework, the strategies for UAV operations
467 need to be further studied. In the framework, UAV (or UAVs) plays a vital role in tracking target and
468 reference objects. Therefore, future studies on how to capture mobile target objects and a stationary
469 reference object simultaneously and continuously must be done. To this end, operating multiple UAVs
470 and realizing real-time image stitching could be considered as a possible solution. Also, thorough field
471 experiments need to be conducted in order to investigate how the elevation of UAV can impact
472 proximity monitoring and prediction performance. The higher elevation a UAV flies at, the wider the
473 scene can be monitored. However, it can cause target objects to be seen too small, which can affect
474 object detection performance and accordingly proximity monitoring and prediction accuracy.

475

476 ***Implications of Using GAN-based DNN for Trajectory Prediction***

477 GAN is basically an unsupervised generative model that makes plausible data from a noise input (e.g.,
478 Gaussian noise) based on probability distribution learned from real data (Goodfellow et al. 2014). The
479 uniqueness of GAN that yields a highly competitive edge over other generative models (e.g., naïve
480 Bayes, hidden Markov model, and Markov random fields) is the adversarial training between generator
481 and discriminator. In GAN training, the generator tries to minimize min-max loss whereas the
482 discriminator counteracts to maximize it (Equation 5). In this min-max game, both generator and
483 discriminator get to improve while competing with each other. This adversarial training is known to
484 better fit to understanding complex distributions of real data (e.g., images and speeches) than using a
485 certain loss (objective) function manually devised.

486

$$\text{Min - Max Loss} = E_x[\log D(x)] + E_z[\log(1 - D(G(z)))] \quad \text{Equation 5}$$

Note: $D(x)$ =discriminator's estimate of the probability that real data instance x is real; E_x =expected value over all real data instances; $G(z)$ =generator's output when given input z ; $D(G(z))$ =discriminator's estimate of the probability that a fake instance is real; E_z =expected value over all inputs to the generator.

487

488 The interesting fact is that the GAN can also be used for trajectory prediction which is basically
489 a supervised learning problem. The S-GAN incorporates the GAN architecture and uses adversarial
490 training so that it can enhance the capability to learn hidden distribution of mobile objects' diverse
491 trajectories. More noticeably, the S-GAN leverages the GAN architecture in a conditional way such that
492 it can still take prior information (i.e., past trajectory) as input and consume ground truth for network
493 supervision. That is, instead of using noise input, it takes past trajectories and initializes the decoder
494 with the prior information, thereby generating future trajectories more conformed to the past. Moreover,
495 it uses L_2 loss (Equation 6) in addition to the min-max loss so that it can condition the decoder to
496 generate the prediction closer to the ground truth. In these ways, the S-GAN could take advantage of
497 both adversarial training and supervised learning, consequently resulting in a promising performance
498 of trajectory prediction.

499

$$L_2 \text{ Loss} = \sum_{i=1}^n (Y_g - Y_p)^2 \quad \text{Equation 6}$$

Note: n=dimension of output vector; Y_g =ground truth trajectory; Y_p =predicted trajectory.

500

501 However, the application of S-GAN presents several challenges, particularly in training. The
502 adversarial training between generator and discriminator can be often stuck at local minima and in
503 general takes a longer period than the training of normal DNNs. The single most important reason
504 behind such challenges is the imbalance between generator and discriminator. For example, if the
505 discriminator is too strong, then the generator training can easily fail due to vanishing gradients. On the
506 other hand, if the generator easily defeats the discriminator, it tends to produce the most plausible output
507 repeatedly, which can make the discriminator permanently trapped (called mode collapse).

508 Compared to dominant DNN architectures such as convolutional neural network (CNN) and
509 recurrent neural network (RNN), GAN is a new kind of DNN. Certainly, there are still many chances
510 to improve its trainability, which may include regularization using noise addition (Arjovsky and Bottou
511 2017), penalization of discriminator weights (Roth et al. 2017), and the use of advanced min-max loss

512 (e.g., *Wasserstein loss*). The application of such advanced techniques would provide us with a better
513 chance to leverage S-GAN (or other GAN-based DNNs) and to have a higher accuracy of proximity
514 prediction thereby.

515 Another way to improve the prediction accuracy would include post-processing incorporating
516 construction-specific knowledge. The S-GAN showed a promising accuracy of trajectory prediction in
517 this study; however, it would not cover all the possible scenarios that can happen on construction sites
518 and the prediction accuracy can deteriorate in those cases. The post-processing incorporating
519 construction-specific knowledge, such as the average or maximum velocity of each robot (or
520 equipment), construction robots' pre-programmed collision avoidance behavior, and construction
521 workers' collision avoidance behavior, can likely be used to refine predicted trajectory's velocity and
522 direction, which could improve the overall accuracy of proximity prediction.

523

524 **Conclusions**

525 In this study, the authors developed a DNN-based framework for proximity prediction, leveraging a
526 camera-mounted UAV, object detection DNN (YOLO-V3) and trajectory prediction DNN (S-GAN).
527 Also, the authors demonstrated the framework's validity in a field test: the framework achieved 0.95
528 meters average proximity error (APE) and 1.71 meters final proximity error (FPE) in predicting 5.28
529 seconds future proximity. During construction operations, contact-driven hazards by mobile robots (or
530 mobile equipment and vehicle) can easily arise in various scenarios: for example, a navigating robot
531 suddenly change in direction or an autonomous vehicle could reverse into a blind spot. In such
532 unpredictable situations, the proximity prediction would enable advance detection of impending
533 collisions, thereby making pro-active interventions possible. Specifically, the predictive functionality
534 would allow robots to make alternative path planning and rerouting beforehand and enable providing
535 advance alerts to workers via wearable devices. These pro-active interventions would contribute to
536 mitigating the chances of impending collisions between mobile robots (or mobile equipment and vehicle)
537 and construction workers. Moreover, the authors apply GAN to trajectory prediction, which opens a
538 new possibility of GAN for potential construction applications.

539 **Data Availability**

540 Some or all data, models, or code that support the findings of this study are available from the
541 corresponding author upon reasonable request.

542

543 **Acknowledgments**

544 The work presented in this paper was supported financially by a National Science Foundation Award
545 (No. IIS-1734266, '*Scene Understanding and Predictive Monitoring for Safe Human-Robot*
546 *Collaboration in Unstructured and Dynamic Construction Environments* '). Any opinions, findings, and
547 conclusions or recommendations expressed in this paper are those of the authors and do not necessarily
548 reflect the views of the National Science Foundation. Lastly, the authors wish to specially thank Weston
549 Tanner, John McGlennon, and Chris Klaft from WALSH Construction Co. and Steve La Cava and
550 Andy Thelen from TOEBE Construction LLC. for their considerate assistance in collecting onsite data.

551

552 **References**

553 Alahi, A., Goel, K., Ramanathan, V., Robicquet, A., Fei-Fei, L., and Savarese, S. 2016. "Social lstm:
554 Human trajectory prediction in crowded spaces." In *Proc., 2016 IEEE Conference on Computer*
555 *Vision and Pattern Recognition.*, 961-971. Las Vegas, NV: IEEE.

556 Antonini, G., Bierlaire, M., and Weber, M. 2006. "Discrete choice models of pedestrian walking
557 behavior." *Transportation Research Part B: Methodological.* 40 (8): 667-687.
558 <https://doi.org/10.1016/j.trb.2005.09.006>.

559 Arjovsky, M., and Bottou, L. 2017. "Towards principled methods for training generative adversarial
560 networks." In *Proc., 5th International Conference on Learning Representations*. Toulon, France.
561 arXiv:1701.04862.

562 Awolusi, I., Marks, E., and Hallowell, M. 2018. "Wearable technology for personalized construction
563 safety monitoring and trending: Review of applicable devices." *Automation in construction*, 85
564 (Jan): 96-106. <https://doi.org/10.1016/j.autcon.2017.10.010>.

565 Bock, T. 2015. "The future of construction automation: Technological disruption and the upcoming

566 ubiquity of robotics." *Automation in Construction.* 59 (Nov): 113-121.

567 <https://doi.org/10.1016/j.autcon.2015.07.022>.

568 Cardno, C. A. 2018. "Robotic Rebar-Tying System Uses Artificial Intelligence." *Civil Engineering Magazine Archive.* 88 (1): 38-39. <https://doi.org/10.1061/ciegag.0001260>.

570 Chen, V. C., Li, F., Ho, S.-S., and Wechsler, H. 2006. "Micro-Doppler effect in radar: phenomenon, 571 model, and simulation study." *IEEE Transactions on Aerospace and electronic systems.* 42 (1): 572 2-21. <https://doi.org/10.1109/TAES.2006.1603402>.

573 Cui, J., Liew, L. S., Sabaliauskaite, G., and Zhou, F. 2019. "A review on safety failures, security attacks, 574 and available countermeasures for autonomous vehicles." *Ad Hoc Networks,* 90 (Jul): 101823. 575 <https://doi.org/10.1016/j.adhoc.2018.12.006>.

576 DuCarme, J. 2019. "Developing effective proximity detection systems for underground coal mines." 577 <https://doi.org/10.1016/B978-0-08-101288-8.00003-1>.

578 Gargoum, S. A., Karsten, L., El-Basyouny, K., and Koch, J. C. 2018. "Automated assessment of vertical 579 clearance on highways scanned using mobile LiDAR technology." *Automation in Construction.* 580 95 (Nov): 260-274. <https://doi.org/10.1016/j.autcon.2018.08.015>.

582 Guiochet, J., Machin, M., and Waeselynck, H. 2017. "Safety-critical advanced robots: A survey." 583 <https://doi.org/10.1016/j.robot.2017.04.004>.

585 Gupta, A., Johnson, J., Fei-Fei, L., Savarese, S., and Alahi, A. 2018. "Social gan: Socially acceptable 586 trajectories with generative adversarial networks." In *Proc., 2018 IEEE Conference on* 587 *Computer Vision and Pattern Recognition.*, 2255-2264. Salt Lake City, UT: IEEE.

588 Helbing, D., and Molnar, P. 1995. "Social force model for pedestrian dynamics." *Physical review E,* 51 589 (5): 4282. <https://doi.org/10.1103/PhysRevE.51.4282>.

590 Kim, D., Goyal, A., Newell, A., Lee, S., Deng, J., and Kamat, V. R. 2019a. "Semantic relation detection 591 between construction entities to support safe human-robot collaboration in construction." *2019* 592 *ASCE International Conference on Computing in Civil Engineering.*, 265-272. Atlanta, GA:

593 ASCE.

594 Kim, D., Liu, M., Lee, S., and Kamat, V. R. 2019b. "Remote proximity monitoring between mobile
595 construction resources using camera-mounted UAVs." *Automation in Construction*. 99 (Mar):
596 168-182. <https://doi.org/10.1016/j.autcon.2018.12.014>.

597 Kim, D., Liu, M., Lee, S., and Kamat, V. R. 2019. "Trajectory prediction of mobile construction
598 resources toward pro-active struck-by hazard detection." In *Proc., International Symposium on
599 Automation and Robotics in Construction.*, 982-988. Banff, AB, Canada.

600 Kim, P., Chen, J., and Cho, Y. K. 2018. "SLAM-driven robotic mapping and registration of 3D point
601 clouds." *Automation in Construction*. 89 (May): 38-48.
602 <https://doi.org/10.1016/j.autcon.2018.01.009>.

603 Lattanzi, D., and Miller, G. 2017. "Review of robotic infrastructure inspection systems." *Journal of
604 Infrastructure Systems*. 23 (3): 04017004. [https://doi.org/10.1061/\(ASCE\)IS.1943-555X.0000353](https://doi.org/10.1061/(ASCE)IS.1943-
605 555X.0000353).

606 Leal-Taixé, L., Fenzi, M., Kuznetsova, A., Rosenhahn, B., and Savarese, S. 2014. "Learning an image-
607 based motion context for multiple people tracking." In *Proc., 2016 IEEE Conference on
608 Computer Vision and Pattern Recognition.*, 3542-3549. Las Vegas, NV: IEEE.

609 Li, J., Wang, Y., Zhang, K., Wang, Z., and Lu, J. 2019. "Design and analysis of demolition robot arm
610 based on finite element method." *Advances in Mechanical Engineering*. 11 (6):
611 1687814019853964. <https://doi.org/10.1177/1687814019853964>.

612 Lin, T.-Y., Maire, M., Belongie, S., Hays, J., Perona, P., Ramanan, D., Dollár, P., and Zitnick, C. L.
613 2014. "Microsoft coco: Common objects in context." In *Proc., European conference on
614 computer vision.*, 740-755. Zurich, Swiss: Springer

615 Liu, J., and Li, G. 2018. "Research on the development of 3D printing construction industry based on
616 diamond model." *Innovative Technology and Intelligent Construction.*, 164-176. Reston, VA:
617 ASCE.

618 Loop, C., and Zhang, Z. 1999. "Computing rectifying homographies for stereo vision." In *Proc., 1999
619 IEEE Computer Society Conference on Computer Vision and Pattern Recognition.*, 125-131.

620 Fort Collins, CO: IEEE.

621 Memarzadeh, M., Golparvar-Fard, M., and Niebles, J. C. 2013. "Automated 2D detection of
622 construction equipment and workers from site video streams using histograms of oriented
623 gradients and colors." *Automation in Construction.* 32 (Jul): 24-37.
624 <https://doi.org/10.1016/j.autcon.2012.12.002>.

625 Moon, S., Becerik-Gerber, B., and Soibelman, L. 2019. "Virtual Learning for Workers in Robot
626 Deployed Construction Sites." *Advances in Informatics and Computing in Civil and*
627 *Construction Engineering.*, 889-895.

628 Park, J., Marks, E., Cho, Y. K., and Suryanto, W. 2015. "Performance test of wireless technologies for
629 personnel and equipment proximity sensing in work zones." *Journal of Construction*
630 *Engineering and Management.* 142 (1): 04015049. [https://doi.org/10.1061/\(ASCE\)CO.1943-7862.0001031](https://doi.org/10.1061/(ASCE)CO.1943-7862.0001031).

632 Park, M.-W., and Brilakis, I. 2012. "Construction worker detection in video frames for initializing vision
633 trackers." *Automation in Construction.* 28 (Dec): 15-25.
634 <https://doi.org/10.1016/j.autcon.2012.06.001>.

635 Pellegrini, S., Ess, A., and Van Gool, L. 2010. "Improving data association by joint modeling of
636 pedestrian trajectories and groupings." In *Proc., European conference on computer vision.* 452-
637 465. Crete, Greece: Springer.

638 Pfeiffer, M., Paolo, G., Sommer, H., Nieto, J., Siegwart, R., and Cadena, C. 2018. "A data-driven model
639 for interaction-aware pedestrian motion prediction in object cluttered environments." In *Proc.,*
640 *2014 IEEE International Conference on Robotics and Automation.*, 1-8. Brisbane, QLD,
641 Australia: IEEE.

642 Redmon, J., and Farhadi, A. 2018. "Yolov3: An incremental improvement." *arXiv preprint*
643 *arXiv:1804.02767*.

644 Research and Markets. 2019. "Global construction robot market - drivers, restraints, opportunities,
645 trends, and forecast up to 2025." (URL: <https://www.researchandmarkets.com>, accessed on
646 Sept. 08 2019)

647 Ruff, T. 2006. "Evaluation of a radar-based proximity warning system for off-highway dump trucks."
 648 *Accident Analysis & Prevention*. 38 (1): 92-98. <https://doi.org/10.1016/j.aap.2005.07.006>.

649 Salimans, T., and Kingma, D. P. 2016. "Weight normalization: A simple reparameterization to accelerate
 650 training of deep neural networks." In *Proc., 30th Conference on Neural Information Processing
 651 Systems.*, 901-909. Barcelona, Spain: NIPS.

652 Tavares, P., Costa, C. M., Rocha, L., Malaca, P., Costa, P., Moreira, A. P., Sousa, A., and Veiga, G. .2019.
 653 "Collaborative Welding System using BIM for Robotic Reprogramming and Spatial
 654 Augmented Reality." *Automation in Construction*. 106 (Oct): 102825.
 655 <https://doi.org/10.1016/j.autcon.2019.04.020>.

656 Tay, M. K. C., and Laugier, C. 2008. "Modelling smooth paths using gaussian processes." In *Proc.,
 657 Field and Service Robotics.*, 381-390.

658 Teizer, J. 2015. "Wearable, wireless identification sensing platform: self-monitoring alert and reporting
 659 technology for hazard avoidance and training (SmartHat)." *Journal of Information Technology
 660 in Construction*. 20 (19): 295-312.

661 Teizer, J., Allread, B. S., Fullerton, C. E., and Hinze, J. 2010. "Autonomous pro-active real-time
 662 construction worker and equipment operator proximity safety alert system." *Automation in
 663 construction*. 19 (5): 630-640. <https://doi.org/10.1016/j.autcon.2010.02.009>.

664 Tractica. 2019. "Construction & demolition robots - robot assistants and structure, finishing, and
 665 infrastructure robots: global market analysis and forecast." (URL:
 666 <https://www.tractica.com/research/construction-demolition-robots>, accessed on Sept. 08 2019)

667 Trautman, P., Ma, J., Murray, R. M., and Krause, A. 2015. "Robot navigation in dense human crowds:
 668 Statistical models and experimental studies of human–robot cooperation." *The International
 669 Journal of Robotics Research*. 34 (3): 335-356. <https://doi.org/10.1177/0278364914557874>.

670 Tsuruta, T., Miura, K., and Miyaguchi, M. 2019. "Mobile robot for marking free access floors at
 671 construction sites." *Automation in Construction*. 107 (Nov): 102912.
 672 <https://doi.org/10.1016/j.autcon.2019.102912>.

673 Vähä, P., Heikkilä, T., Kilpeläinen, P., Järvi, M., and Gamba, E. 2013. "Extending automation

674 of building construction—Survey on potential sensor technologies and robotic applications."
675 *Automation in Construction*. 36 (Dec): 168-178. <https://doi.org/10.1016/j.autcon.2013.08.002>.

676 Varghese, J. Z., and Boone, R. G. 2015. "Overview of autonomous vehicle sensors and systems." In
677 *Proc., International Conference on Operations Excellence and Service Engineering*., 178-191.

678 Vega-Heredia, M., Mohan, R. E., Wen, T. Y., Siti'Aisyah, J., Vengadesh, A., Ghanta, S., and Vinu, S.
679 2019. "Design and modelling of a modular window cleaning robot." *Automation in*
680 *Construction*. 103 (Jul): 268-278. <https://doi.org/10.1016/j.autcon.2019.01.025>.

681 Wang, M.-z., Luo, M., Cen, Y.-w., and Huang, J.-z. 2018. "Research on Space Pose and Hydraulic
682 System Stability of Remote-Controlled Demolition Robot." In *Proc., 5th International*
683 *Conference on Information Science and Control Engineering*., 962-967.

684 Więckowski, A. 2017. "'JA-WA"-A wall construction system using unilateral material application with
685 a mobile robot." *Automation in Construction*. 83 (Nov): 19-28.
686 <https://doi.org/10.1016/j.autcon.2017.02.005>.

687 Xu, Y., Piao, Z., and Gao, S. 2018. "Encoding crowd interaction with deep neural network for pedestrian
688 trajectory prediction." In *Proc., IEEE Conference on Computer Vision and Pattern Recognition*.,
689 5275-5284. Salt Lake City, UT: IEEE.

690 Yamaguchi, K., Berg, A. C., Ortiz, L. E., and Berg, T. L. 2011. "Who are you with and where are you
691 going?" In *Proc., IEEE Conference on Computer Vision and Pattern Recognition*., 1345-1352.
692 Colorado Springs, CO: IEEE.

693 Yang, Y., Pan, M., and Pan, W. 2019. "Co-evolution through interaction'of innovative building
694 technologies: The case of modular integrated construction and robotics." *Automation in*
695 *Construction*. 107 (Nov): 102932. <https://doi.org/10.1016/j.autcon.2019.102932>.

696 Yu, S. N., Lee, S. Y., Han, C. S., Lee, K. Y., and Lee, S. H. 2007. "Development of the curtain wall
697 installation robot: Performance and efficiency tests at a construction site." *Autonomous Robots*.
698 22 (3): 281-291.

699

700

701

Table 1. *ADE/FDE* of tuned trajectory prediction models (unit: meters)

Sampling interval (unit: seconds)	Observation length (unit: seconds)		
	2.64	3.96	5.28
0.17	0.85/1.70	0.76/1.63	0.87/1.93
0.33	0.88/1.83	0.45/0.88	0.55/1.14
0.66	0.67/1.38	0.45/0.79	0.45/0.81
1.33	0.80/1.59	0.68/1.07	0.56/0.89

702 *Note: left/right values are ADE/FDE, respectively; ADE/FDE in this table are average values of worker,
703 wheel loader, and excavator; prediction lengths of all the models are 5.28 seconds.*

704

Table 2. *ADE* and *FDE* for truck and worker (unit: meters)

Category	<i>ADE</i>		<i>FDE</i>	
	Worker	Truck	Worker	Truck
Movement pattern #1	1.76	1.84	3.06	2.32
Movement pattern #2	1.44	1.58	2.42	2.21
Movement pattern #3	1.73	2.54	4.68	4.45
Overall	1.64	1.99	3.39	2.99

705 *Note: prediction length=5.28 seconds; ADEs and FDEs in this table are the average values for the three
706 trials; overall values are the average for three movement patterns.*

707

Table 3. *APE* and *FPE* between truck and worker (unit: meters)

Category	<i>APE</i>	<i>FPE</i>
Movement pattern #1	0.44	0.81
Movement pattern #2	1.23	1.94
Movement pattern #3	1.18	2.37
Overall	0.95	1.71

708 *Note: prediction length=5.28 seconds; APES and FPEs in this table are the average values for the three
709 trials; overall values are the average for three movement patterns.*

710

711

712

713

714

715

716

717

718

719

720

721

722

723

724

725

726 **Figure Captions**

727 **Figure 1.** Proximity prediction using a camera-mounted UAV and DNNs

728 **Figure 2.** Module 1: trajectory observation via object detection and coordinate rectification

729 **Figure 3.** Module 2: trajectory prediction using S-GAN

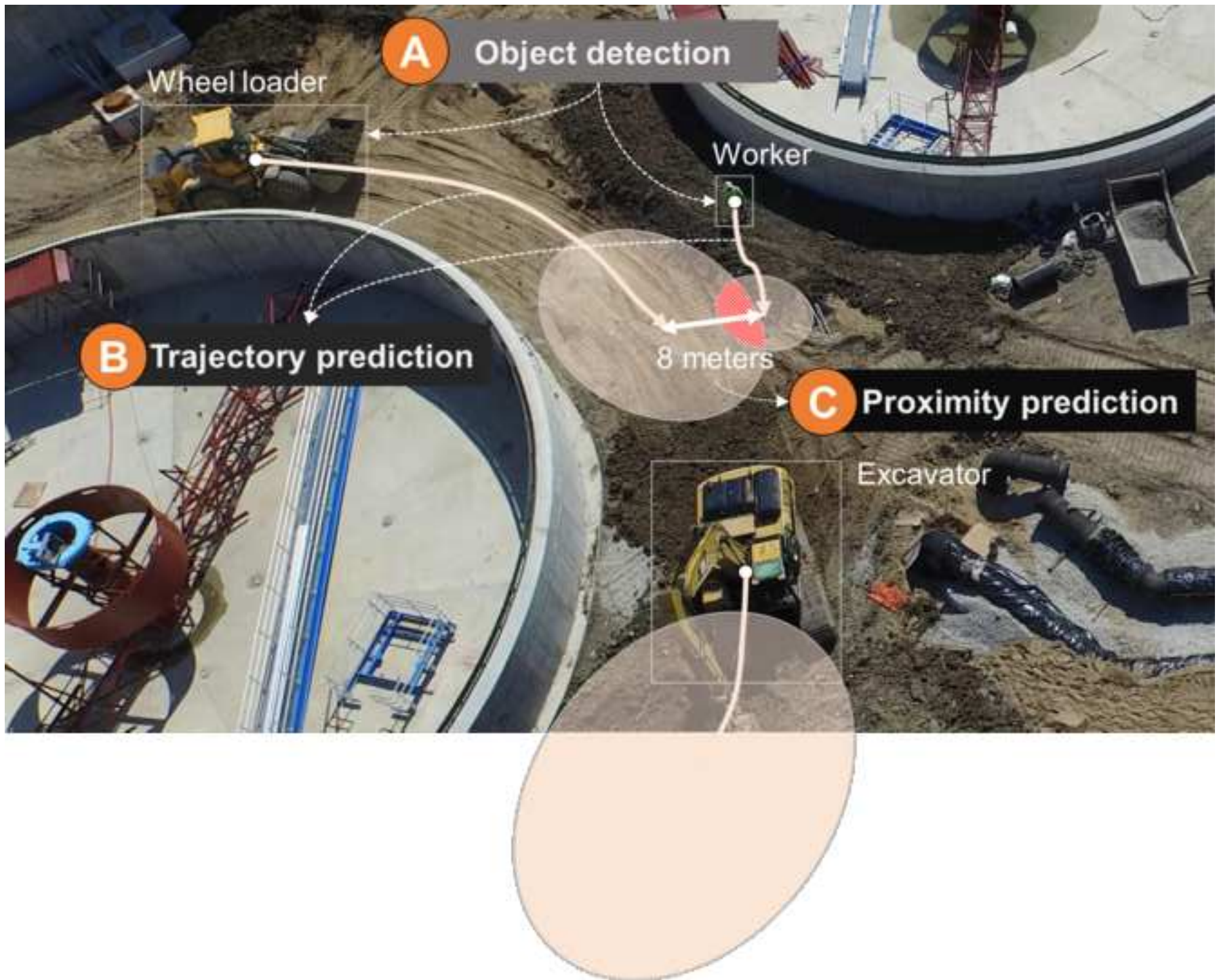
730 **Figure 4.** Network architecture of S-GAN

731 **Figure 5.** Trajectory prediction models' test dataset and evaluation metric (DE: displacement error, unit:
732 meters)

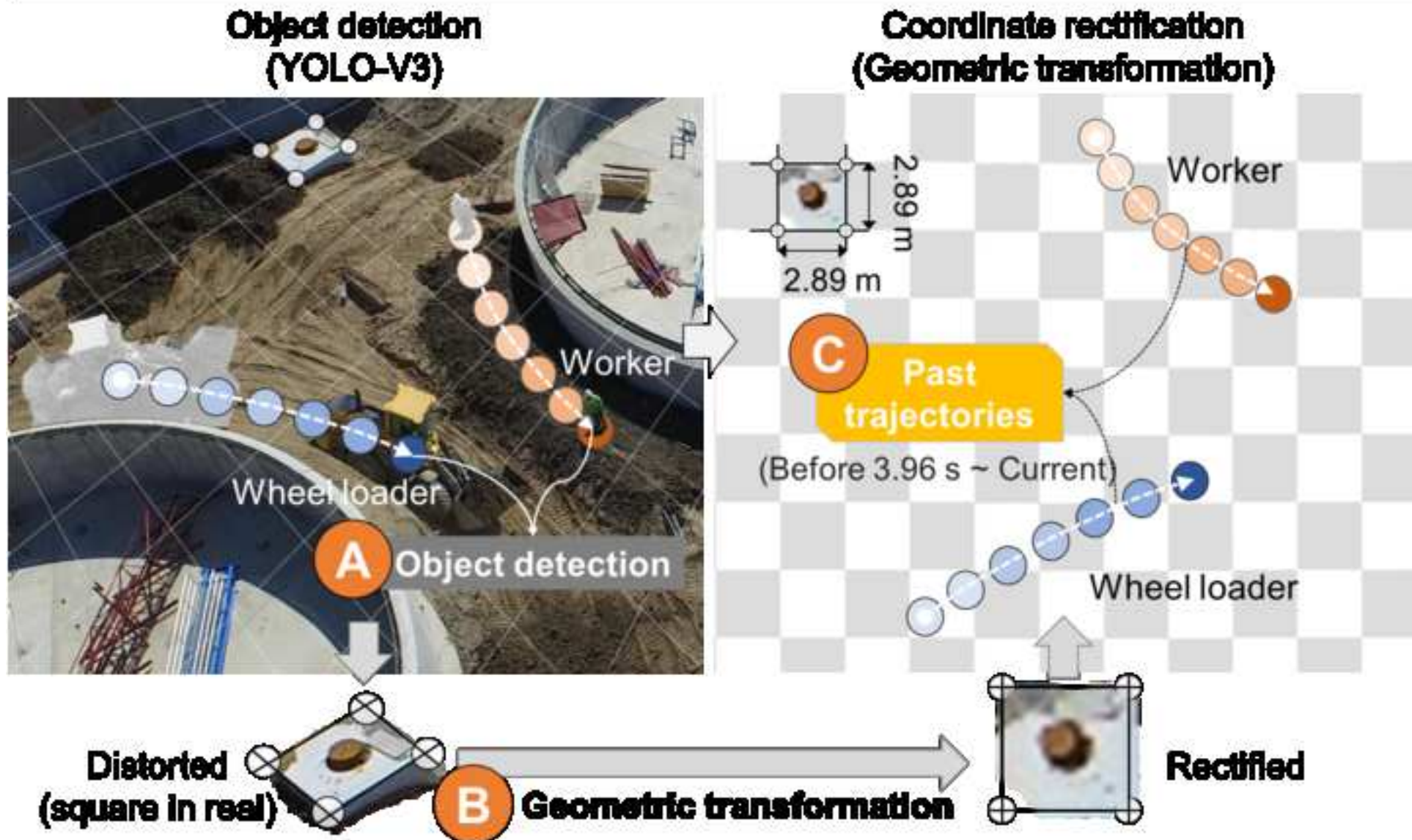
733 **Figure 6.** Field test settings

734 **Figure 7.** Trend of proximity error as prediction time-step increases

735 **Figure 8.** Operating time of Modules 1 and 2



Module 1: Trajectory Observation



Module 2: Trajectory Prediction

Trajectory prediction
(S-GAN)

